

Effect of neutron composition and excitation energy of primary fragments on isospin observables in multifragmentation

D.V. Shetty, A.S. Botvina*, S.J. Yennello, A. Keksis, E. Martin, and G.A. Souliotis

Cyclotron Institute, Texas A&M University,

College Station, Texas 77843, USA

(Dated: November 17, 2018)

Abstract

The isospin properties of primary and secondary fragments produced in multifragmentation of Fe + Ni and Fe + Fe systems with respect to Ni + Ni system are analyzed within the statistical multifragmentation model framework. The reduced neutron and proton densities show an asymmetry in the primary fragments, that is lessened after secondary decay. With increasing isospin (N/Z) this effect increases, while the sensitivity of fragment isospin toward excitation energy and N/Z of the primary fragments remains unchanged.

PACS numbers: 25.70.Lm, 25.70.Mn, 25.70.Pq

arXiv:nucl-ex/0401012v1 12 Jan 2004

* On leave from Institute for Nuclear Research, 117312 Moscow, Russia.

I. INTRODUCTION

Recently, the importance of the isospin degree of freedom in obtaining information regarding charge equilibration and the symmetry dependent terms of the nuclear equation of state has prompted measurements of the isotopic distributions of emitted particles in multifragmentation process [1, 2, 3, 4, 5, 6, 7, 8, 9]. These particles, when emitted, have a broad range of isospin content and carry important information regarding the evolution of the isospin (N/Z) degree of freedom. In multifragmentation, the system quickly expands into the vacuum and decays into hot primary fragments. These hot fragments, despite their short life, carry a significant amount of information about the early stages of the reaction. The surface properties of the primary fragments may provide information about the critical temperature of nuclear matter [10, 11], whereas their isospin is related to the symmetry term in the fragment (nuclear liquid) phase [12, 13]. Similar hot nuclei are also produced in physical processes, such as the collapse of massive stars following supernova II explosions [14], where they can live for a long time in equilibrium with the surrounding nuclear matter.

Experimentally, the observed fragments result from the secondary decay of the hot primary fragments. The secondary decay smears out some of the relevant information making it difficult to study any isospin effect that would have been present before the secondary decay. It is important to verify the extent to which isospin information is preserved in the experimentally measured fragment observables. Therefore, a self-consistent theoretical calculation of primary and secondary fragments, which includes a comparison to many experimental observables, is necessary. Also, the secondary de-excitation process proceeds in physical conditions different from the standard de-excitation of a compound nucleus at low excitation energies: the primary fragments are in the Coulomb field of other fragments. The structure of their excited levels can thus be different. These difficulties regarding the secondary de-excitation can be overcome by comparing the same observables in two similar reactions that differ mainly in isospin asymmetry (see e.g.[1]). Such an observable can also be constructed from the model calculation and compared with experimental results. In a previous study [15], assuming statistical equilibrium in an excited nuclear system, reduced ('free') neutron (ρ_n) and proton (ρ_p) densities were obtained from the measured isotope and isotone yield ratios. It was shown that ρ_n and ρ_p depend significantly on the beam energy, and therefore, may carry information about evolution of fragment isospin with excitation

energy. In this work, we show that the secondary decay decreases the asymmetry in the reduced neutron and proton densities and that this effect is larger for system with higher isospin. The decay, however, still preserves the sensitivity of the neutron content of fragments toward the excitation energy and N/Z of the total system. The observed asymmetry can be well accounted for by the statistical multifragmentation model (SMM) [16].

II. EXPERIMENT

The measurements were performed at the Cyclotron Institute of Texas A&M University (TAMU) using beams provided by the K500 Superconducting Cyclotron. Isotopically pure beams of ^{58}Ni and ^{58}Fe at 30, 40 and 47 MeV/nucleon were bombarded on self-supporting ^{58}Ni (1.75 mg/cm²) and ^{58}Fe (2.3 mg/cm²) targets. Six discrete particle telescopes placed inside a scattering chamber and centered at laboratory angles of 10°, 44°, 72°, 100°, 128° and 148°, were used to measure fragments from the reactions. Each telescope consisted of a gas ionization chamber (IC) followed by a pair of silicon detectors (Si-Si) and a CsI scintillator detector, providing three distinct detector pairs (IC-Si, Si-Si, and Si-CsI) for fragment identification. Further details of the experimental setup and analysis can be found in refs. [15, 17]. The present study is carried out for fragments detected at 44 degrees in the laboratory system, which corresponds to the center of mass angle ≈ 90 degrees. The fragments detected at this angle originate predominantly from central events. Analysis with QMD+SMM model carried out in Ref. [17] supports this conclusion. Nevertheless, a possible admixture of the projectile/target fragmentation processes will be accounted in the following analysis.

III. RATIOS OF REDUCED NUCLEON DENSITIES

In the Grand-Canonical approach for the multifragmentation process (see e.g. [16, 18, 19, 20]), the yield for an isotope with neutron number, N, and proton number, Z (the mass number $A = N + Z$), can be written as

$$Y(N, Z) \propto V \rho_n^N \rho_p^Z Z_{N,Z}(T) A^{3/2} e^{B(N,Z)/T} \quad (1)$$

where V is the volume of the system, $\rho_n \propto e^{\mu_n/T}$ and $\rho_p \propto e^{\mu_p/T}$ are the primary 'free'

neutron and proton densities, respectively. μ_n and μ_p are the neutron and proton chemical potentials. $Z_{N,Z}(T)$ is the intrinsic partition function of the excited fragment. $B(N, Z)$ is the ground state binding energy of the corresponding fragment, and T is the temperature. In the above formula, the effect of the Coulomb interaction on fragment yields is disregarded. In addition, nuclear systems are finite, and this fact influences the fragment yields, especially at low excitation energies [16]. By introducing ρ_n and ρ_p the actual isotope yields are reduced to the approximation appropriate for the thermodynamical limit at high excitation energies [16], and hence referred to as the 'reduced' densities.

By taking ratios of isotope yields of two different systems, one can essentially decrease the uncertainties in the individual isotope yields which exist both in experimental measurements and their theoretical descriptions. In this way, the study of the isotopic composition of the fragments can be reduced to determine the relative neutron and proton densities obtained from the ratios of measured isotopes. The expression for the relative neutron density is

$$\frac{Y(N+k, Z)/Y^{Ni}(N+k, Z)}{Y(N, Z)/Y^{Ni}(N, Z)} = \left(\frac{\rho_n}{\rho_n^{Ni}}\right)^N, \quad (2)$$

where k corresponds to the different isotopes used to determine the double ratio, and Y^{Ni} is the yield for the Ni + Ni reaction. A similar expression for the relative proton density can also be defined. Fig. 1 shows the average ratios of reduced neutron and proton densities as a function of the beam energy for Fe + Ni and Fe + Fe systems. The different symbols in the figure correspond to densities obtained for $k = 1$, $k = 2$ and $k = 3$. One observes a steady decrease in the neutron density and a rise in the proton density with increasing beam energy for the Fe + Ni system. The effect is stronger for Fe + Fe system, having higher N/Z.

IV. EVALUATION OF PARAMETERS OF THE THERMAL SOURCES

In order to compare the results of Fig.1 with the statistical multifragmentation model, the initial parameters of the thermal source, such as the mass (A), charge (Z) and excitation energy (E^*), were evaluated by performing a dynamical BNV calculation [21]. For example, for Fe + Ni central collisions the parameters obtained for the three beam energies were $E_s^* \approx 5, 7$ and 9.4 MeV/nucleon, $A_s \approx 111$, $Z_s \approx 52$. In all cases the N/Z ratios of the sources are approximately the same as in interacting nuclei. These results were obtained at a

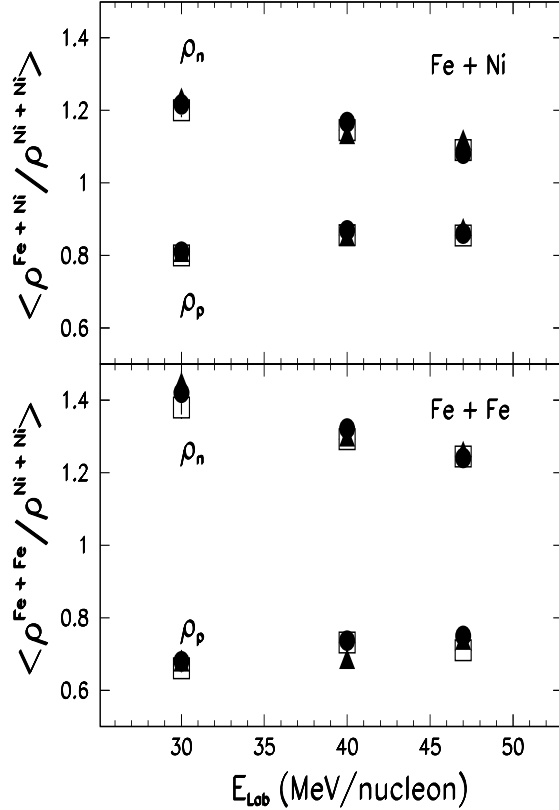


FIG. 1: Relative reduced neutron and proton densities as a function of bombarding energy for Fe + Ni and Fe + Fe reactions. The errors bars are of the size of symbols. The different symbols are explained in the text.

time around 40-50 fm/c after the projectile fuses with the target nuclei, and the quadrupole moment of the nucleon coordinates (used for identification of the deformation of the system) approaches zero. We mention that in the calculations, the form of single sources oscillates and they do not undergo dynamical disintegration into fragments. Consequently, there is no dynamical flow produced in these reactions.

Alternatively, the thermal source parameters can also be estimated from other experimental data. For example, in Ref. [22], for nearly symmetric central collisions of Xe + Sn, excitation energies of $E^* \approx 5$ MeV/nucleon at 32 MeV/nucleon, and $E^* \approx 7$ MeV/nucleon at 50 MeV/nucleon were obtained. It was shown in this work that the SMM describes the disassembly of these nuclear systems into fragments quite well, and reproduces the excitation energies of the observed primary fragments. However, in this case of heavy systems a radial

flow of ≈ 2 MeV/nucleon was identified at 50 MeV/nucleon beam energy. In the present case, the systems are nearly twice as small and more stable with respect to excitation and flow. As supported by experimental observations (see e.g. [23]), small systems produced in central collisions accumulate smaller radial flow than the large systems, consequently, a larger part of their available energy can be transformed into thermal excitation.

V. SMM CALCULATION

The SMM calculation was performed for different sources in order to cover the uncertainties of the thermal source parameters. In particular, we selected ‘complete fusion’ sources: $A_s = 116$, with $Z_s = 52, 54$, and 56 , at excitation energies of $E_s^* = 6, 8$, and 10 MeV/nucleon. In order to account for a possible loss of nucleons during pre-equilibrium emission, and investigate the sensitivity of the results toward the source size, we have also considered the sources $A_s = 58$, with $Z_s = 26, 27$, and 28 . The small sources can also simulate the effects of a two source admixture that leads to the observable isospin characteristics. We have used the standard parameters for the SMM calculations, where the freeze-out density is taken as $1/3$ of the normal nuclear density. This parametrization, together with the adopted secondary de-excitation procedure [20], provide a reasonably good description of the experimental data, including the isotope production (see e.g. [2, 24, 25]). We believe that our analysis of the reduced neutron and proton densities is not very sensitive to the previously mentioned difficulties related to the treatment of secondary de-excitation processes: Since these densities are obtained by averaging over a large number of isotopes, the results are not affected by the rare isotopes which are produced with small probabilities.

In Fig. 2 we show the mean characteristics of the hot primary fragments produced after disintegration of the thermal sources in the freeze-out volume. We show their relative yields, internal excitation energies and N/Z ratios. Even at the lowest E_s^* the systems undergo intensive multifragmentation, characterized by an exponential-like mass distribution. As expected, with increasing excitation the sources break-up into smaller fragments. At $E_s^* = 6$ AMeV the internal excitations of the fragments are around 3 MeV/nucleon, and they increase slightly with their masses. This trend exists because the microcanonical calculation conserves energy: the channels with production of large fragments have smaller Q-values, and, consequently, higher temperatures. In case of canonical calculations, when the tem-

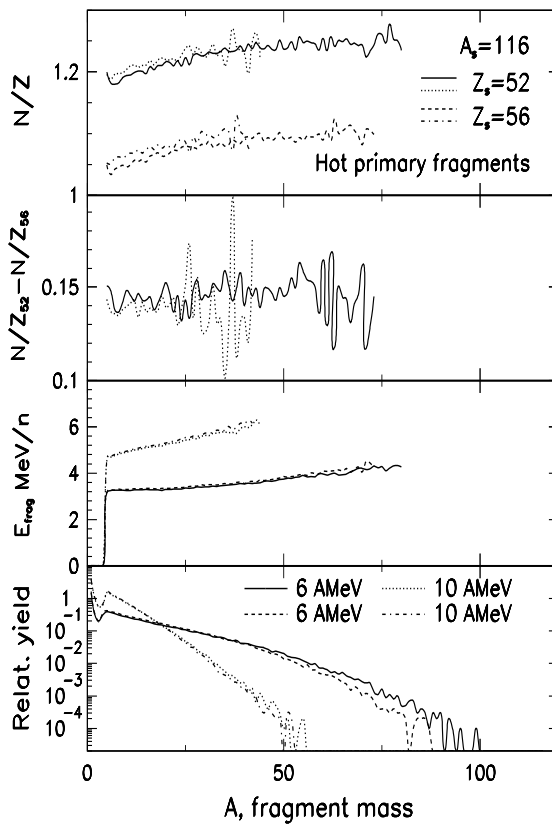


FIG. 2: Characteristics of hot primary fragments versus their mass number A , produced in the freeze-out volume during multifragmentation of the thermal sources with mass number $A_s = 116$, and charges $Z_s = 52$ and $Z_s = 56$, at excitation energies $E_s^* = 6$ and 10 MeV/nucleon (see notations in the figure). Panels from top to bottom: neutron to proton (N/Z) ratio; difference of N/Z ratios between neutron rich ($Z_s = 52$) and neutron poor ($Z_s = 56$) sources at different E_s^* ; internal excitation energies; relative mass yields.

perature is the same for all channels, the internal excitation energies per nucleon would be nearly the same for all fragments having the same level density structure. With increasing E_s^* the internal excitation of fragments increases by ~ 1.5 MeV/nucleon. By comparing the sources with different neutron content, we see that the main difference is in the N/Z ratios of primary fragments. However, these N/Z ratios change only slightly with the excitation energies. They are mainly determined by the N/Z of the sources (actually they are only slightly less than the sources' ratios), and they demonstrate a well-known statistical trend: The N/Z of fragments increases with their mass number [26], which can be explained by the

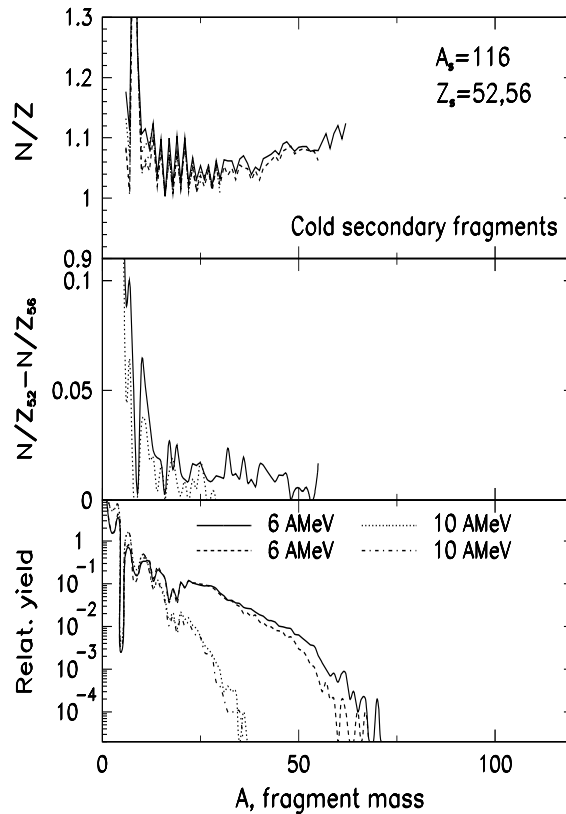


FIG. 3: The same as in Fig. 2, but without the internal excitation panel, for the cold fragments produced after the secondary de-excitation.

Bethe-Weizsaecker formula. Most of the neutrons of the system are accumulated in the hot fragments, the share of free primary neutrons is rather small. However, if we take the difference between the N/Z of fragments in neutron rich and neutron poor sources, we see that it becomes slightly less for the high E_s^* . In particular, the difference of $(N/Z)_{52} - (N/Z)_{56}$ taken between the cases of $E_s^* = 6$ and 10 AMeV and averaged for fragments with $A = 6-20$, is 0.0051, i.e., the share of free neutrons increases a little bit with the excitation energy.

The secondary de-excitation of hot fragments changes their properties. Fig. 3 shows the N/Z ratios and relative yields obtained for the final cold fragments. Both masses and neutron content of fragments decrease considerably. The decrease in the N/Z ratio is due to higher neutron evaporation probability compared to those for the protons. The N/Z of light fragments vary with Z , reflecting their shell structure. However, as one can see from the middle panel, the qualitative difference between the N/Z ratios of hot fragments produced

by sources with different isospin at the same excitation preserves after the secondary de-excitation, though it becomes smaller. Moreover, one can see that the solid and dotted lines in the middle panel are more distinguished than in the Fig. 2. The average difference between the cases with the two excitations increases up to 0.0168 for the fragments $A = 6-20$. This means that the difference of the N/Z of fragments produced in neutron rich and neutron poor sources decreases more for the high excitation energy, as a result of more intensive secondary de-excitation.

VI. COMPARISON OF THE RELATIVE DENSITIES WITH SMM CALCULATION

We now compare the measured relative reduced neutron and proton densities for the Fe + Ni and Fe + Fe systems with the calculation. The properties of fragments discussed above are manifested in the evolution of these densities. Fig. 4 shows the relative densities plotted as a function of excitation energy of the source undergoing fragmentation. The excitation energies were obtained from the BNV calculations carried out for various beam energies. The error bars for the excitation energies corresponds to the two different equation of state used in the BNV calculation, namely, the asy-stiff and the asy-soft equation of state. The regions between solid lines shown in Fig. 4 are the SMM calculation of the densities obtained from the secondary fragment distribution. The regions between dotted lines correspond to the densities calculated from the primary fragment distribution. The width of the two regions represents the measure of sensitivity of the calculation to the assumed source size, i.e. for the sources with $A_s = 58$ and $A_s = 116$. The SMM calculations fit the experimental trends quite well, demonstrating a smooth decrease in ρ_n/ρ_n^{Ni} with increasing excitation energy. Both large- and small-size sources show very similar behavior indicating that the uncertainty of the source size does not influence the overall trends.

The calculation suggests the following interpretation of the data. The main difference in the relative densities is obviously caused by the difference of the N/Z of the sources. It is largest for the Fe + Fe case. The important observation is the decreasing of this difference with the excitation energy, demonstrated in [15]. In fact two effects contribute to it. The first one is a small decreasing of the difference between the N/Z ratios of primary fragments produced by the neutron-rich and neutron-poor sources with the excitation energy. This is

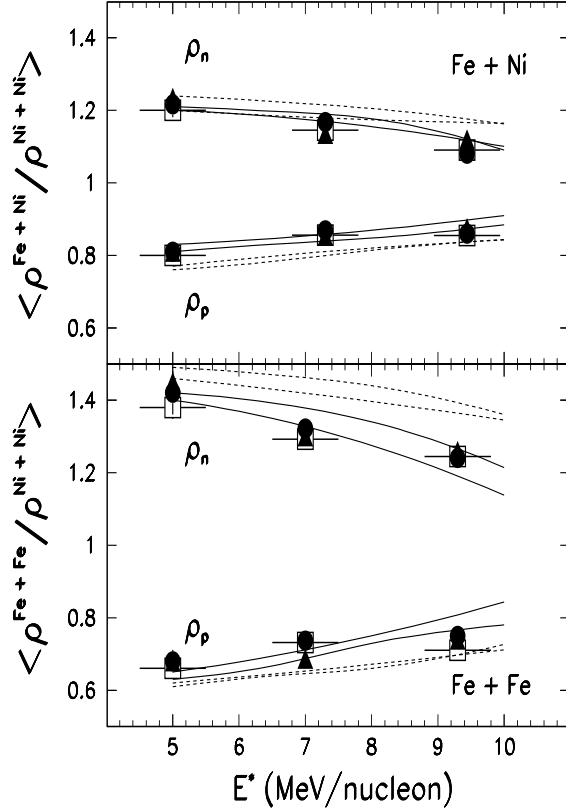


FIG. 4: Relative reduced neutron and proton densities as a function of excitation energy for Fe + Ni and Fe + Fe reactions. The errors bars for the excitation energy is explained in the text. The different (solid and dotted) regions correspond to the statistical model calculations as discussed in the text.

because for high E_s^* more neutron rich primary fragments are produced, however, if the small clusters are already neutron rich, free neutrons are predicted. Nevertheless, the secondary de-excitation is very important, since it changes drastically the N/Z of fragments. In the case of a larger internal excitation of fragments, the secondary decay produces more similar cold fragments, despite the difference in their initial N/Z ratios. This leads to decreasing of ρ_n/ρ_n^{Ni} (and the corresponding increasing ρ_p/ρ_p^{Ni}), observed in the experiment.

VII. CONCLUSION

We have explained the observed evolution of the fragment isospin with the excitation energy in the framework of the SMM. This is consistent with the following picture of the reaction: The primary fragments produced at the freeze-out density in the central collisions are excited and usually contain more neutrons than observed in cold fragments. Moreover, their N/Z ratio is only slightly less than the N/Z ratio of the excited nuclear systems. In our cases, the internal excitation energy of the primary fragments increases with the total excitation energy of the system. Therefore, the secondary de-excitation of fragments becomes more efficient in removing neutrons from fragments, and, the difference of the primary N/Z ratios disappears gradually with excitation energy, for the final cold fragments. However, these characteristics of primary fragments (their internal excitation energies and N/Z ratios), and the observed isospin evolution, are obtained for very high excitation energies, when the initial compound nucleus dissociates completely into small fragments. The isospin of fragments produced at energies near the multifragmentation threshold may behave differently [26]. We believe that the present results demonstrate that the properties of hot fragments can be effectively estimated by investigating general trends of cold fragments versus the excitation energy and the neutron richness of the sources.

VIII. ACKNOWLEDGMENT

The authors wish to thank the staff of the Texas A&M Cyclotron facility for the excellent beam quality. This work was supported in part by the Robert A. Welch Foundation through grant No. A-1266, and the Department of Energy through grant No. DE-FG03-93ER40773. One of the authors (ASB) thanks Cyclotron Institute TAMU for hospitality and support.

-
- [1] H. Xu et al., *Phys. Rev. Lett.* **85**, 716 (2000).
 - [2] P. M. Milazzo, *Phys. Rev. C* **62**, 041602 (2000).
 - [3] M. B. Tsang, W. A. Friedman, C. K. Gelbke, W. G. Lynch, G. Verde, and H. S. Xu, *Phys. Rev. C* **64**, 041603 (2001).
 - [4] M. B. Tsang et al., *Phys. Rev. C* **64**, 054615 (2001).

- [5] M. B. Tsang et al., Phys. Rev. C **66**, 044618 (2002).
- [6] S. J. Yennello et al., Phys. Lett. B **321**, 15 (1994).
- [7] H. Johnston et al., Phys. Lett. B **371**, 186 (1996).
- [8] H. Johnston et al., Phys. Rev. C **56**, 1972 (1997).
- [9] D. Rowland et al., Phys. Rev. C **67**, 064602 (2003).
- [10] R. Ogul and A. S. Botvina, Phys. Rev. C **66**, 051601 (2002).
- [11] V. A. Karnaukhov et al., Phys. Rev. C **67**, 011601 (2003).
- [12] A. S. Botvina, O. V. Lozhkin, and W. Trautmann, Phys. Rev. C **65**, 044610 (2002).
- [13] A. Ono et al., Phys. Rev. C **68**, 051601 (2003).
- [14] H. A. Bethe, Rev. Mod. Phys. **62**, 801 (1990).
- [15] D. V. Shetty, S. J. Yennello, E. Martin, A. Keksis, and G. A. Souliotis, Phys. Rev. C **68**, 021602 (2003).
- [16] J. P. Bondorf, A. S. Botvina, A. S. Iljinov, I. N. Mishustin, and K. Sneppen, Phys. Rep. **257**, 133 (1995).
- [17] E. Ramakrishnan et al., Phys. Rev. C **57**, 1803 (1998).
- [18] J. Randrup and S. Koonin, Nucl. Phys. A **356**, 223 (1981).
- [19] S. Albergo et al., Nuovo Cimento A **89**, 1 (1985).
- [20] A. S. Botvina et al., Nucl. Phys. A **475**, 663 (1987).
- [21] V. Baran, M. Colonna, M. D. Toro, V. Greco, M. Z. Pfabe, and H. H. Wolter, Nucl. Phys. A **703**, 603 (2002).
- [22] S. Hudan et al., Phys. Rev. C **67**, 064613 (2003).
- [23] B. Hong et al., Phys. Rev. C **57**, 244 (1998).
- [24] A. S. Botvina et al., Nucl. Phys. A **584**, 737 (1995).
- [25] E. M. Winchester et al., Phys. Rev. C **63**, 014601 (2001).
- [26] A. S. Botvina and I. N. Mishustin, Phys. Rev. C **63**, 061601 (2001).